ISSN (Print) 1226-1750
ISSN (Online) 2233-6656
Journal of Magnetics 26(4), 410-414 (2021) https://doi.org/10.4283/JMAG.2021.26.4.410

Co^{2+} Distribution and the Related Magnetic Evolution in Ca-substituted Spinel $CoFe_2O_4$

Kwang Joo Kim[1], Jongho Park[1], and Jae Yun Park[2]*

[1]*Department of Physics, Konkuk University, Seoul 05029, Korea*
[2]*Department of Materials Science and Engineering, Incheon National University, Incheon 22012, Korea*

(Received 10 October 2021, Received in final form 14 December 2021, Accepted 14 December 2021)

Magnetic properties of cobalt ferrites with a portion of Co^{2+} ions being replaced by Ca^{2+} were investigated by vibrating-sample magnetometry (VSM). The $Ca_xCo_{1-x}Fe_2O_4$ ($x \leq 0.2$) specimens were prepared as thin films by a sol-gel deposition method. According to the VSM results, the saturation magnetization (M_S) of the Ca-substituted ferrite decreased from that of $CoFe_2O_4$ proportional to the Ca composition x. Raman spectral analyses revealed that the Ca-substituted ferrites had a lower tetrahedral Co^{2+} population in the spinel lattice compared to $CoFe_2O_4$. The decreasing trend of M_S is consistent with the result of theoretical evaluation in which the relative population of Co^{2+} ions among the tetrahedral and octahedral sites is proportional to the relative Raman scattering intensities of 615 and 470 cm^{-1} peaks, respectively.

Keywords : ferrite, calcium, thin film, Raman scattering, magnetic properties

1. Introduction

Ferrimagnetic $CoFe_2O_4$ has been under extensive research for potential applications such as microwave absorption [1], magnetic resonance imaging [2], and magneto-mechanical sensing [3]. In crystallography, $CoFe_2O_4$ belongs to the spinel group in which Co^{2+} and Fe^{3+} cations occupy either the 8a (tetrahedral) or the 16d (octahedral) sites surrounded by four and six O^{2-} anions at the 32e sites, respectively. The population of Co^{2+} and Fe^{3+} ions among the tetrahedral (A) and octahedral (B) sites is likely to vary for different fabrication processes [4-7].

For ferrimagnetic $CoFe_2O_4$, the majority of Co^{2+} ions tend to occupy the B sites rather than the A sites. The ferrimagnetism has been explained in terms of the competition between anti-parallel A and B magnetic moments. $CoFe_2O_4$ in its perfect inverse-spinel state would have 50 % of Fe^{3+} ions occupying the A sites, while the other 50 % of Fe^{3+} ions and all Co^{2+} ions would occupy the B sites. The octahedral Co^{2+} population can be expressed using an inversion parameter δ [8] that is described as $(Co^{2+}_{1-\delta}\ Fe^{3+}_{\delta})^{A}[Co^{2+}_{\delta}\ Fe^{3+}_{2-\delta}]^{B}O_4$, in which $\delta = 1$ for the perfect inverse-spinel $CoFe_2O_4$. Experimental studies on $CoFe_2O_4$ have suggested that a finite portion of the Co^{2+} ions must occupy the A sites. The physical and chemical properties of $CoFe_2O_4$ are likely to vary with the value of δ.

In this work, the effects of calcium (Ca) substitution in the spinel lattice on the structural and magnetic properties of cobalt ferrites ($Ca_xCo_{1-x}Fe_2O_4$) were investigated. Substitution of other metallic elements has been adopted for tailoring the intrinsic properties of the ferrites such as magnetic hysteresis and electromagnetic absorption [1, 9-11]. Ca atom (atomic number = 20) has [Ar] $4s^2$ electronic configuration, thus, the ionized Ca^{2+} in $Ca_xCo_{1-x}Fe_2O_4$ must have no $3d$ electron, while Co and Fe ions have $3d$ electrons. The octahedral preference of Ca^{2+} ions in the spinel lattice is likely to alter the distribution of Co^{2+} and Fe^{3+} ions among the A and B sites, affecting the physical properties of the cobalt ferrites.

The $Ca_xCo_{1-x}Fe_2O_4$ specimens were prepared as thin films by a sol-gel method. The structural properties of the specimens were investigated by X-ray diffraction (XRD), Raman spectroscopy, and X-ray photoelectron spectroscopy (XPS). The magnetic hysteresis curves of the specimens were investigated by vibrating sample magnetometry (VSM). The magnetic evolution of $Ca_xCo_{1-x}Fe_2O_4$ is discussed in comparison with that of Sc-substituted $Sc_xCoFe_{2-x}O_4$.

*Corresponding author: Tel: +82-32-835-8271
Fax: +82-32-835-0778, e-mail: pjy@inu.ac.kr

2. Experimental

$Ca_xCo_{1-x}Fe_2O_4$ specimens with $x \leq 0.2$ were prepared as thin films through a sol-gel deposition process. Precursor solution was prepared by dissolving $Fe(NO_3)_3 \cdot 9H_2O$ and $Co(CH_3COO)_2 \cdot 4H_2O$ together in 2-methoxyethanol (20 ml) and ethanolamine (2 ml) at 170 ºC. For Ca doping $Ca(NO_3)_2 \cdot 4H_2O$ was added. Spin-coating of the precursor solution was done on Si(100) substrate rotating 3000 rpm for 20 s followed by heating at 300 ºC for 5 min. This process was repeated to increase the thickness of the gel film. Post-annealing of the gel film was done at 800 ºC for 4 h in air to obtain solid-state ferrite film.

XRD (Cu K_α line, wavelength = 0.15418 nm) measurements were performed on the ferrite specimens to figure out crystal structure under a grazing-incidence condition with fixed X-ray incidence angle of 4º. Raman scattering measurements using a diode laser (wavelength = 514 nm, power = 1 mW) were performed to investigate vibrational modes in the ferrites. XPS measurements using Al K_α line (photon energy = 1486.7 eV) were performed to confirm the existence of Ca in the ferrites. Magnetic hysteresis curves of the ferrites were obtained from VSM measurements under the condition that the external magnetic field was applied parallel to the film's plane and varied in the ± 15 kOe range.

3. Results and Discussion

The Ca ions in the Ca-doped specimens can be identified by XPS on Ca 2*p* electrons. As shown in Fig. 1, the binding energy (BE) peaks of $2p_{3/2}$ and $2p_{1/2}$ electrons of Ca^{2+} ion are located at 346.8 and 350.4 eV, respectively. The spin-orbit splitting of 3.6 eV for the Ca^{2+} ion turns out to be smaller by 0.7 eV than that of Sc^{3+} ion [12], which is located next to Ca in the periodic table.

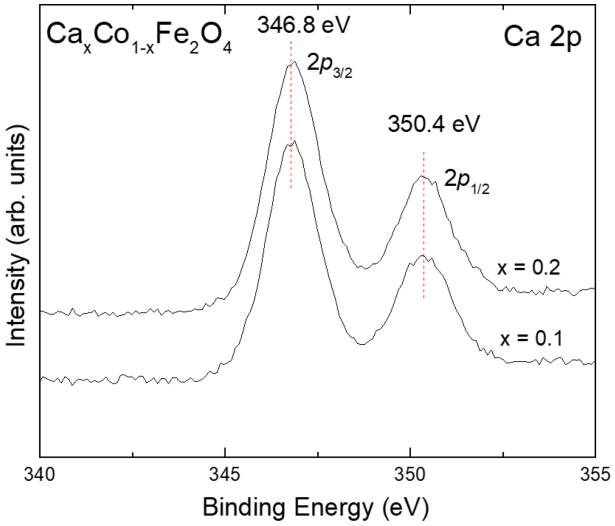

Fig. 1. (Color online) X-ray photoelectron spectra of Ca 2*p* electrons of $Ca_xCo_{1-x}Fe_2O_4$ specimens.

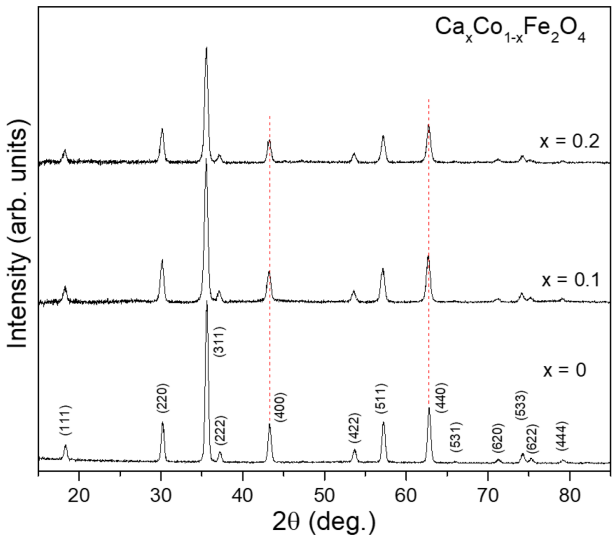

Fig. 2. (Color online) X-ray diffraction patterns of $Ca_xCo_{1-x}Fe_2O_4$ specimens.

The XRD patterns of the $Ca_xCo_{1-x}Fe_2O_4$ specimens are quite alike to that of $CoFe_2O_4$ as shown in Fig. 2. The estimated lattice constants of the specimens are close to 0.836 nm. Considering the octahedral preference of Ca^{2+} ion, the XRD investigation implies that Ca^{2+} ions exist in the B sites without any significant distortion of the spinel lattice. The XRD patterns suggest that the $Ca_xCo_{1-x}Fe_2O_4$ specimens contain no secondary phases up to $x = 0.2$.

In Fig. 3, magnetic hysteresis loops of the $Ca_xCo_{1-x}Fe_2O_4$ specimens measured by using VSM are shown in comparison with that of $CoFe_2O_4$ [13]. A magnetic hysteresis

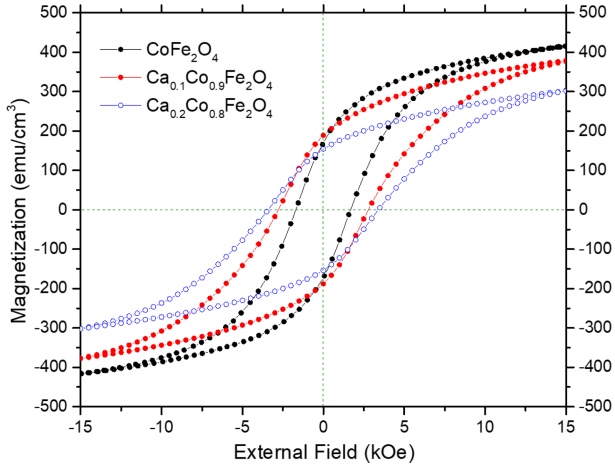

Fig. 3. (Color online) Magnetic hysteresis loops of $Ca_xCo_{1-x}Fe_2O_4$ specimens.

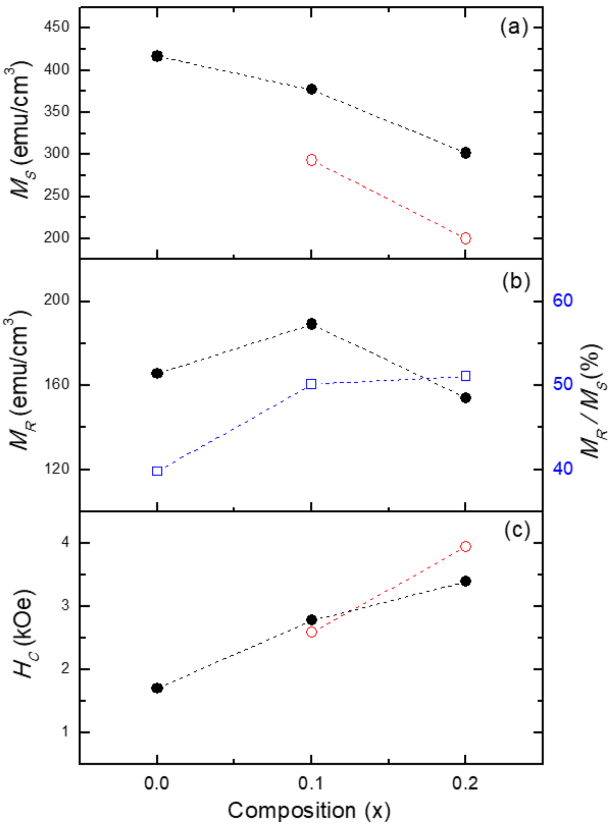

Fig. 4. (Color online) Magnetic parameters of $Ca_xCo_{1-x}Fe_2O_4$ specimens: (a) saturation magnetization (M_S), (b) remanence (M_R), and (c) coercivity (H_C).

loop used to be characterized by saturation magnetization (M_S), remanence (M_R), and coercivity (H_C). The variations of M_S, M_R, and H_C for the specimens are exhibited (filled circles) in Figs. 4(a), 4(b), and 4(c), respectively. For the Ca-doped specimens, M_S decreases but H_C increases with increasing Ca composition compared to those of $CoFe_2O_4$. The increase of H_C is seen to be inversely proportional to M_S.

The relation between H_C and M_S can be described using the magnetic anisotropy constant (K) as $H_CM_S = (0.96)K$, where H_C and M_S have units of Oe and G (= $(4\pi)^{-1}$ emu/cm^3), respectively, and K has the unit of J/m^3. The relation was based on a homogeneous rotation coercivity model [14] that was applied to explain the relation between H_C and M_S for nanocrystalline Li-ferrites. The values of K for the Ca-doped specimens obtained from the equation are 8.8×10^4 and 8.5×10^4 J/m^3 for $x = 0.1$ and 0.2, respectively, while it is 5.9×10^4 J/m^3 for $CoFe_2O_4$. The Ca-doped specimens showing the smaller magnetization turn out to have the larger magnetic anisotropy than $CoFe_2O_4$.

In Fig. 4(b), the squareness ratio (M_R/M_S) is also shown (open squares) along with the M_R data (filled circles). As the Ca composition increases, the hysteresis curves

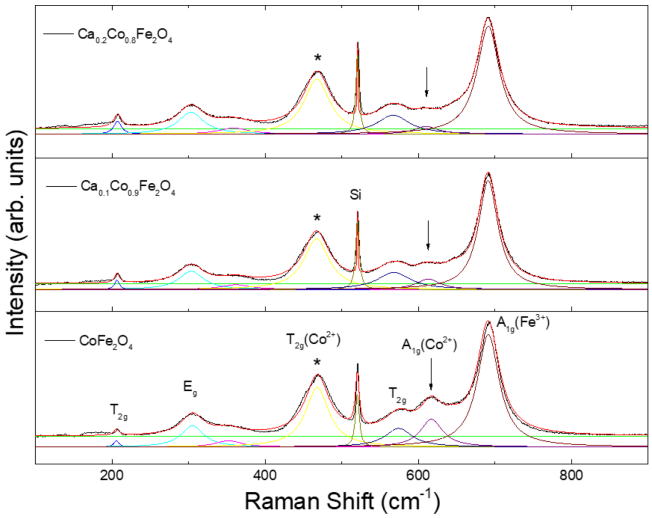

Fig. 5. (Color online) Raman spectra of $Ca_xCo_{1-x}Fe_2O_4$ specimens (black line). Colored curves below the experimental curve represent the result of curve-fitting.

become more square-like with increasing demagnetization. The squareness ratio reaches to 0.5 for the Ca-doped specimens, implying that the domains are randomly oriented in the demagnetized state [14].

In Fig. 5, Raman scattering spectra (black line) of the Ca-doped specimens are shown in comparison with $CoFe_2O_4$. The distinction in the Raman spectra of the Ca-doped specimens compared to $CoFe_2O_4$ is a reduction in the intensity of a peak near 615 cm^{-1} compared to those near it as indicated by arrows. It is interpreted as due to an A_{1g} vibrational mode for symmetric stretching of tetrahedral O^{2-} ions surrounding the A site [15, 16].

In the Raman spectra of ferrimagnetic Fe_3O_4 above 600 cm^{-1}, single A_{1g} peak is observed near 670 cm^{-1} [17], while two peaks are observed near 615 and 693 cm^{-1} in those of $CoFe_2O_4$. The 693 cm^{-1} peak is ascribed to $A_{1g}(Fe^{3+}\text{-}O^{2-})$ mode at the tetrahedral Fe^{3+} ion, while the 615 cm^{-1} peak is ascribed to $A_{1g}(Co^{2+}\text{-}O^{2-})$ mode at the tetrahedral Co^{2+} ion [15].

The Raman peaks located below 600 cm^{-1} for $CoFe_2O_4$ have been ascribed to T_{2g} (580, 470, 207 cm^{-1}) and E_g (305 cm^{-1}) vibrational modes corresponding to symmetric and anti-symmetric bending of octahedral O^{2-} ions, respectively [16]. Especially, the peak near 470 cm^{-1} looks strong for $CoFe_2O_4$ [15, 16], while it is absent in the Raman spectrum of Fe_3O_4 [17, 18]. So, it is ascribed to T_{2g} mode related to octahedral Co^{2+} ion. Thus, the Raman spectra of $Ca_xCo_{1-x}Fe_2O_4$ contain phonon modes ascribed to both tetrahedral (615 cm^{-1}) and octahedral (470 cm^{-1}) Co^{2+} ions. The intensity ratio between the 615 cm^{-1} and 470 cm^{-1} peak can be an indicative of the relative population of Co^{2+} ions between the A and B

sites. The peak appeared at 520 cm^{-1} is due to the Si substrate of the specimen.

The relative Co^{2+} population at the A and B sites of the $Ca_xCo_{1-x}Fe_2O_4$ specimens was estimated by curve-fitting the Raman spectra, as shown in Fig. 5, to get the areal ratio between the 615 cm^{-1} (I_A) and 470 cm^{-1} (I_B) peaks. For the $Ca_xCo_{1-x}Fe_2O_4$ specimens the intensity ratio (I_A:I_B) turned out to be 16:84 and 11:89 for x = 0.1 and 0.2, respectively, while it is 30:70 for $CoFe_2O_4$. The result implies that A site occupancy of Co^{2+} ions in $Ca_xCo_{1-x}Fe_2O_4$ is reduced compared to $CoFe_2O_4$.

Assuming all the Ca^{2+} ions occupy the B sites, the ionic distribution in $Ca_xCo_{1-x}Fe_2O_4$ among the A and B sites can be described as $(Co^{2+}_{1-\delta}\,Fe^{3+}_{\delta})^{A}[Co^{2+}_{\delta-x}\,Ca_x\,Fe^{3+}_{2-\delta}]^{B}O_4$. Then, the value of δ can be estimated using the Raman intensity ratios to be 0.86 and 0.91 for x = 0.1 and 0.2 of $Ca_xCo_{1-x}Fe_2O_4$, respectively, while δ = 0.70 for $CoFe_2O_4$ (x = 0). The resultant octahedral Co^{2+} composition ($\delta - x$) becomes 0.76 and 0.71 for x = 0.1 and 0.2, respectively, while the tetrahedral Co^{2+} composition ($1 - \delta$) becomes 0.14 and 0.09, respectively. Thus, the octahedral Co^{2+} composition in $Ca_xCo_{1-x}Fe_2O_4$ turns out to increase compared to $CoFe_2O_4$ (0.70), while the tetrahedral Co^{2+} composition turns out to decrease compared to $CoFe_2O_4$ (0.30).

The estimated magnetic moments per formula unit based on $(Co^{2+}_{1-\delta}\,Fe^{3+}_{\delta})^{A}\,[Co^{2+}_{\delta-x}\,Ca^{2+}_{x}\,Fe^{3+}_{2-\delta}]^{B}O_4$ is 3.3 μ_B and 2.8 μ_B for x = 0.1 and 0.2, respectively, where the contribution of Co^{2+}, Fe^{3+} and Ca^{2+} are 3 μ_B, 5 μ_B, and 0, respectively. Comparing with the estimated magnetic moment of 4.2 μ_B for $CoFe_2O_4$ based on $(Co^{2+}_{1-\delta}\,Fe^{3+}_{\delta})^{A}\,[Co^{2+}_{\delta-x}\,Fe^{3+}_{2-\delta}]^{B}O_4$ with δ = 0.70, the magnetic moment of $Ca_xCo_{1-x}Fe_2O_4$ is reduced to 79 % and 67 % of that of $CoFe_2O_4$, for x = 0.1 and 0.2, respectively. When the values of M_S in Fig. 4(a) obtained from the experimental hysteresis curves are compared, the magnetic moment of $Ca_xCo_{1-x}Fe_2O_4$ is reduced to 90 % and 72 % of that of $CoFe_2O_4$. Thus, the theoretical estimation based on the octahedral preference of Ca^{2+} ions in $Ca_xCo_{1-x}Fe_2O_4$ can explain the decreasing trend of M_S with increasing Ca composition in the spinel oxide.

In Figs. 4(a) and 4(c), the M_S and H_C of $Ca_xCo_{1-x}Fe_2O_4$ (filled circles) are compared with those of $Sc_xCoFe_{2-x}O_4$ (open circles) in ref. 12. Scandium atom (atomic number = 21) is located next to calcium atom in the periodic table having one d electron with [Ar] $3d^1\ 4s^2$ electronic configuration. For Sc has ionic preference of +3 in spinel oxides, $Sc_xCoFe_{2-x}O_4$ can be a stable compound in which Sc^{3+} ion replaces Fe^{3+} ion. The values of M_S of $Sc_xCoFe_{2-x}O_4$ are only 70 % (x = 0.1) and 66 % (x = 0.2) of those of $Ca_xCo_{1-x}Fe_2O_4$, while the values of H_C of $Sc_xCoFe_{2-x}O_4$ are rather close to those of $Ca_xCo_{1-x}Fe_2O_4$.

4. Conclusions

The effects of octahedral Ca^{2+} ions on the Co^{2+} distribution among the tetrahedral and octahedral sites and the magnetic hysteresis in spinel $Ca_xCo_{1-x}Fe_2O_4$ ferrite have been studied using VSM, Raman scattering, XRD, and XPS. The Raman spectral analyses reveal a reduction of tetrahedral Co^{2+} population through the octahedral occupation of Ca^{2+} ions. The magnetic hysteresis data of $Ca_xCo_{1-x}Fe_2O_4$ show gradual reduction of M_S with increasing x. The theoretical magnetic moments per formula unit of $Ca_xCo_{1-x}Fe_2O_4$ estimated by comparing the intensities of Raman scattering modes involving tetrahedral and octahedral Co^{2+} ions reveal a decreasing trend with increasing x in agreement with that of M_S.

Acknowledgment

This work was supported by Incheon National University Research Grant in 2019.

References

[1] D. Mandal and K. Mandal, J. Magn. Magn. Mater. **536**, 168127 (2021).
[2] M. M. Yallapu, S. F. Othman, E. T. Curtis, B. K. Gupta, M. Jaggi, and S. C. Chauhan, Biomaterials **32**, 1890 (2011).
[3] N. Somaiah, T. V. Jayaraman, P. A. Joy, and D. Das, J. Magn. Magn. Mater. **324**, 2286 (2012).
[4] P. Kumar, S. K. Sharma, M. Knobel, and M. Singh, J. Alloys Comp. **508**, 115 (2010).
[5] A. Thampi, K. Babu, and S. Verma, J. Alloys Comp. **564**, 143 (2013).
[6] R. C. Kambale, P. A. Shaikh, C. H. Bhosale, K. Y. Rajpure, and Y. D. Kolekar, Smart Mater. Struct. **18**, 115028 (2009).
[7] S. Laureti, G. Varvaso, A. M. Testa, D. Fiorani, E. Agostinelli, G. Piccaluga, A. Musinu, A. Ardu, and D. Peddis, Nanotechnology **21**, 315701 (2010).
[8] P. Chandramohan, M. P. Srinivasan, S. Velmurugan, and S. V. Narasimhan, J. Solid State Chem. **184**, 89 (2011).
[9] K. Ugendar, V. Vaithyanathan, L. N. Patro, S. S. R. Inbanathan, and K. K. Bharathi, J. Phys. D: Appl. Phys. **49**, 305001 (2016).
[10] S. Agrawal, A. Parveen, and A. Azam, J. Magn. Magn. Mater. **414**, 144 (2016).
[11] S. Joshi, M. Kumar, S. Chhoker, A. Kumar, and M. Singh, J. Magn. Magn. Mater. **426**, 252 (2017).
[12] K. J. Kim, J. Park, and J. Y. Park, J. Magn. **25**, 453 (2020).

[13] K. J. Kim and J. Park, J. Sol-Gel Sci. Technol. **92**, 40 (2019).
[14] H. Yang, Z. Wang, L. Song, M. Zhao, J. Wang, and H. Luo, J. Phys. D: Appl. Phys. **29**, 2574 (1996).
[15] R. S. Yadav, I. Kuritka, J. Vilcakova, J. Havlica, J. Masilko, L. Kalina, J. Tkacz, J. Svec, V. Enev, and M. Hajduchova, Adv. Nat. Sci.: Nanosci. Nanotechnol. **8**, 045002 (2017).
[16] R. Nongjai, S. Khan, K. Asokan, H. Ahmed, and I. Khan, J. Appl. Phys. **112**, 084321 (2012).
[17] O. N. Shebanova and P. Lazor, J. Solid State Chem. **174**, 424 (2003).
[18] K. J. Kim, T. Y. Koh, J. Park, and J. Y. Park, J. Magn. **22**, 360 (2017).